MJFAS
Malaysian Journal of Fundamental and Applied Sciences

Nurani *et al.* | Malaysian Journal of Fundamental and Applied Sciences, Vol. 22 (2026) 974–990

RESEARCH ARTICLE

A Dual-Functional *Color-Shiftable* Ion Imprinted Polymer for Visual Detection and Online Preconcentration of Trace Cu^{2+}

Dita Arifa Nurani[a,b], Untung Triadhi[a], Dian Ayu Setyorini[a], Muhammad Bachri Amran[a]*

[a]Analytical Chemistry Research Group, Faculty of Mathematics and Natural Sciences, Institut Teknologi Bandung, Ganesha 10, Bandung 40116, Indonesia, [b]Chemistry Department, Faculty of Mathematics and Natural Sciences, Universitas Indonesia, Pondok Cina, Depok 16424, Indonesia

Abstract A dual-functional Cu-Ion Imprinted Polymer (Cu-IIP) was prepared using a facile imprinting method as a color-responsive adsorbent for simultaneous visual detection and selective online preconcentration of trace Cu^{2+} ions. Cu-IIP was obtained by bulk polymerization using the chromophore ligand 4-pyridylazo resorcinol (PAR), the functional monomer 4-vinyl pyridine, the crosslinker ethylene glycol dimethacrylate (EGDMA), the porogen methanol, and the initiator benzoyl peroxide (BPO) under mild condition (T 65 ^{o}C) for 2h. The synthesized imprinted polymers exhibited a maximum adsorption capacity of 67.32 mg. g^{-1} for Cu^{2+} ions. Adsorption equilibrium followed Langmuir isotherm model (R^2 0.9883), indicating homogeneous binding sites. The pseudo-second-order kinetic model (R^2 0.9999) most accurately represents kinetic data, indicating significant chemical interactions between the metal ions and the sorbent. The thermodynamic parameters confirmed that the adsorption process is both spontaneous and exothermic ($\Delta G < 0$). The Cu-IIP was integrated into an online Flow Injection Analysis (FIA) coupled with flame atomic absorption spectrometry (FIA-FAAS). The method showed a good linearity from 100-1000 μg. L^{-1} with R^2 0.9919, a detection limit (LoD) of 3.07 μg. L^{-1}, a LoQ of 9.03 μg. L^{-1}, a preconcentration factor of 2.2, and a good precision 3.53%. Application of Cu-IIP-FIA-FAAS system to a water sample demonstrated high accuracy, with recovery values 102.9-105.5%. In addition, the incorporation of PAR demonstrated a distinct concentration-dependent color change, highlighting its dual functionality as both a selective sorbent and a colorimetric sensing material for monitoring trace Cu^{2+} in environmental water.

Keywords: Ion imprinted polymer, PAR, copper, flow injection analysis (FIA), DIC analysis.

Introduction

***For correspondence:**
amran@itb.ac.id

Received: 06 June 2026
Accepted: 24 August 2026

© Copyright Nurani. This article is distributed under the terms of the Creative Commons Attribution License, which permits unrestricted use and redistribution provided that the original author and source are credited.

Copper is among the most prevalent heavy metal contaminants in aquatic environments [1]. The issue is a global concern due to its toxicity, potential for bioaccumulation, and significant adverse effects on the aquatic ecosystem. Bioaccumulation over an extended period causes serious adverse health effects [2,3]. High levels of copper exposure can damage the liver and kidneys [4]. The World Health Organization (WHO) has established a maximum permissible limit of 2.0 mg. L^{-1} for copper (Cu^{2+}) ions in drinking water. In comparison, the U.S. Environmental Protection Agency (EPA) has implemented a stricter limit of 1.3 mg. L^{-1} for Cu^{2+}[5]. Therefore, the removal and monitoring of Cu^{2+} from environmental water are of great importance.

Generally, Cu is primarily detected by FAAS, which offers lower cost, good response quality, and easy operation compared to other methods. However, matrix interferences limited the direct determination of Cu in water samples by FAAS. Prior to Cu^{2+} analysis, a sample pretreatment is required to remove matrix components and enrich a Cu^{2+} in samples. Several adsorbents have been used for the Cu^{2+} adsorption such as silica gel [6,7], activated carbon [8,9], resin [10], and carbon nanotubes [11,12]. The performance of these materials was influenced by the nature of the sorbents, whereas the conventional sorbents with

or without metal-complexing agent functionalization have poor selectivity [13]. Ion-imprinted polymers (IIPs) are commonly known as selective sorbents, which have specific functional cavities of target ions based on coordination number, shape, size, and charges [14,15]. IIPs were easy to prepare and exhibit high chemical and physical stability without reducing their affinity for target ions [16].

In IIPs synthesis, polymerizable complexing agents play a crucial role, as they directly influence the sorbents' selectivity performance [17]. Several studies have investigated the synthesis of IIPs for Cu^{2+} separation [13,14,18,19]. 4-Pyridilazo resorcinol (PAR) is a chromogenic chelating agent that contributes to the alteration of the color in the sorbent and exhibits various degrees of color intensity following metal adsorption [20]. Furthermore, previous research reported that azo based ligands such as DPC and PAR enhance selectivity toward Cu^{2+} [21–23]. Possible species of Cu-PAR complex were $CuHL_2$ and CuL_2 at pH above 6.75 [24]. The presence of specific binding sites and appropriately sized cavities for Cu^{2+} ions on the polymers surface enhances selectivity and adsorption efficiency for Cu^{2+} ions via metal−ligand interactions [25]. Moreover, 4-VP, the functional monomer, can chelate Cu^{2+} and give strong imprinting sites towards the template ion [26]. The immobilization of non-vinyl ligands, or a combination of non-vinyl and vinyl ligands, facilitates the formation of binary or ternary complexes with metal ions within the polymer matrix [27].

Unlike the traditional IIP that primarily focuses on adsorption, this study incorporates a chromogenic recognition Cu-IIP within the imprinted matrix. In this research, Cu-IIP was synthesized by trapping a non-vinyl ligand (PAR) to form ternary complexes of metal ion with 4-VP. This ternary complex enhances the selectivity and binding capacity of IIPs for target ions [28,29].

The integration of IIP into Flow Injection Analysis (FIA) systems would be effective for online preconcentration of trace metal ions. To the best of current knowledge, the direct integration of color-responsive ion imprinted polymer into FIA system represents a novel approach, as it has not been reported in the literature. FIA offers advantages such as low chemicals use, good reproducibility, high sampling throughput, and easy automation [30,31]. Metal specific IIP sorbents integrated with the FIA system enhance control over mass transfer and the interaction time of the analyte with the cavity sites, leading to improved reproducibility and faster analysis compared to traditional batch or offline SPE methods [30].

This study used the bulk polymerization method for IIP synthesis due to its simplicity, high monomer conversion, and the production of a highly crosslinked structure [32] using EGDMA as a crosslinker, BPO as an initiator, and methanol as a solvent. The effect of pH, contact time, and maximum adsorption capacity were also determined. The adsorption performance as a function of pH, contact time, adsorption thermodynamics of Cu^{2+} alongside the adsorption isotherm were also studied. For online preconcentration, Cu-IIP was used as a packed bed in a mini column integrated with a FIA system prior to FAAS measurement. In addition, a digital image colorimetry (DIC) analysis was performed to assess the capability of Cu-IIP to produce a measurable color change upon the adsorbing of Cu^{2+}. The present investigation demonstrates the feasibility of Cu-IIP as a dual-functional material for selective preconcentration and optical detection.

Materials and Methods

Materials

$Cu(CH_3COO)_2.H_2O$ was purchased from Fisher Scientific. 4,2-pyrydilazo resorcinol (PAR) and benzoyl peroxide (BPO) were obtained from Merck, ethylene glycol dimethacrylate (EGDMA), methanol (CH_3OH), 4-vinyl pyridine, NaOH, and HNO_3 were procured from Sigma Aldrich. High purity materials and reagents were employed throughout the study.

Apparatus

The concentration of Cu ions was analyzed using a double-beam flame atomic absorption spectrometer (GBC Avanta 6506). The pH meter (Mettler-Toledo) was used to measure the pH of the solution. Fourier Transform Infrared (FTIR) Prestige-21 (Shimadzu, Japan) (at wavenumber 4000-400 cm^{-1}) was employed to obtain the FTIR spectra of IIPs. The morphology of the polymers was evaluated with a scanning electron microscope (SEM), Hitachi High-Technologies Corporation SU-3500, Japan, equipped with eZAP smart quant. Before analysis, synthesized polymers were mounted on a carbon holder and coated with gold using the ion sputtering MC-1000 (Hitachi High-Technologies Corporation). A reciprocating shaker bath OVAN was used for the sorption experiment. The FIA system consists of a peristaltic pump (Masterflex L/S Cole Parmer Instrument Company) and Tygon tubing to circulate the

sample, carrier solution, and eluent. An 8-way valve (Vici Valco) controls the injection process. A mini column (length = 3 cm diameter = 1.2 mm) was used to pack the sorbents. The PowerChrome software (ADInstruments) is employed to record the FIAgram.

Preparation of the Cu-IIP

The synthetic route of Cu-IIP is illustrated in **Figure 1**. 0.1 mmol $Cu(CH_3COO)_2.H_2O$ was dissolved in 10 mL methanol, and 0.1 mmol of PAR was added dropwise to the Cu^{2+} solution with continuous stirring at T 298K for 60 min to ensure the equilibration of the complex reaction (Cu: PAR 1/1). Then 4 mmol 4-VP, 40 mmol EGDMA and 150 mg BPO were added to the mixture solution and stirred for 2 h. This mixture was sonicated for 10 min and bubbled with N_2 gas for 10 min. The solution was heated in an oil bath at 65ºC for 2 h.

The IIPs particles underwent repeated filtration and washing with methanol and water to remove residual monomers and crosslinker. The polymers were dried for 24 hours until the constant weight was achieved. Subsequently, the products were ground and sieved to obtain particles of 60-80 mesh size. The particles were treated with 5.0 mol. L^{-1} HNO_3 to ensure complete removal of the template ion. The final products were washed with deionized water until the pH was neutral, then dried in an oven at 100 °C. For comparison, a non-imprinted polymer (NIP) and functionalized ligand (NIPL) were synthesized under the similar conditions without adding the templates Cu^{2+}.

Adsorption experiments

Copper ions adsorption from aqueous solutions was evaluated through batch experiments. In the static adsorption study, a specified amount of IIPs was equilibrated with a known concentration of Cu^{2+} standard solution. A 20 mg Cu-IIP were added in 25 mL Cu^{2+} standard solutions in a 50 mL reaction vessel at specified temperatures (298, 308 and 318 K). After being continuously shaken for 60 min at 120 rpm, the solutions were then filtered using filter paper 101 with a diameter 11 cm.

For the pH test, 20 mg of IIPs were added to 25 mL of a standard Cu^{2+} solutions (10 mg. L^{-1}) at varying pH levels. The initial pH of standard Cu^{2+} solutions was adjusted within 2.0-9.0 using 0.01 M HNO_3 and 0,01 M NaOH solution.

The influence of the initial concentration of Cu^{2+} on IIPs adsorption capacity was also evaluated. 20 mg of IIPs were immersed in 25 mL of standard Cu^{2+} solutions at different concentrations (5, 10, 25, 50, 100, and 200 mg.L^{-1} at optimum contact time and pH. The amount of Cu^{2+} adsorbed on IIPs was measured by FAAS. The adsorption capacity (qe) was calculated using the following equation (eq.1):

$$qe = \frac{(C_o - C_e) \times V}{m} \qquad (1)$$

Where C_o and C_e is the initial concentration and concentration of Cu^{2+} at equilibrium state (mg. L^{-1}), V is the volume of solution (L), and m is the sorbents mass (g).

The Langmuir, Freundlich, and Temkin adsorption isotherm models were the primary models used to evaluate the adsorption behaviors of adsorbents. The isothermal adsorption experiments were carried out using a series of Cu^{2+} solutions at concentration range 5.0 to 200.0 mg. L^{-1}. The adsorption kinetics were performed using 10 mg. L^{-1} of Cu^{2+} solution. After shaking for a certain time (10, 30,60, 90, 120 and 180 min), the sorbents were separated by filter paper, and the residual Cu^{2+} concentration in the filtrate was analyzed by FAAS.

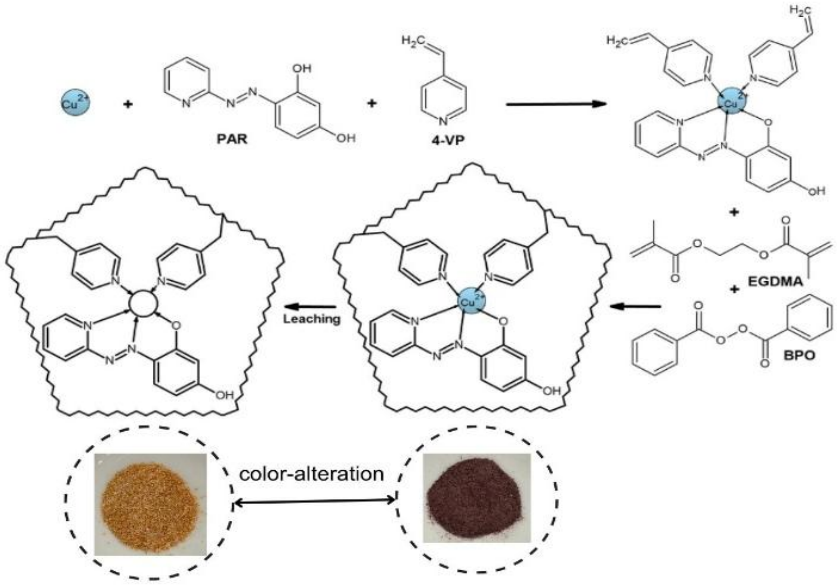


Figure 1. The synthetic route of Cu-IIP.

Selectivity

The selective adsorption capacity of Cu-IIP was evaluated by determining the equilibrium concentrations of 1x10^{-4} M Cu^{2+} and the interfering ions Pb^{2+}, Cd^{2+}, and Zn^{2+}.The experiments were performed in the quaternary mixture. The distribution coefficient (K_d) and selectivity coefficient (k) were determined by the following equation [14]:

$$K_d = \frac{(C_o - C_e)}{C_e} \; x \; \frac{V}{m} \qquad (2)$$

$$k = \frac{K_{d\,Cu^{2+}}}{K_{d\,M^{2+}}} \qquad (3)$$

C_i and C_f is the he initial concentration and concentration of Cu^{2+} at equilibrium state (mg. L^{-1}), V is the volume of the solution, and m is the weight of synthesized polymer (g).

Online preconcentration analysis by Cu-IIP FIA-FAAS system

The schematic scheme of the online preconcentration system based on Cu-IIP integrated with FIA-FAAS is shown in **Figure 2**. A 20 mg of Cu-IIP was packed into mini column (length = 3 cm, d = 1.2 mm). To prevent any leakage, the mini column was sealed with PTFE tape. Deionized water at pH 6 was employed as the carrier solvent, while 0.5 mL of 3.0 M HNO_3 was used as eluent. A 1 mL sample was injected into the FIA system at a constant flow rate of 2.0 mL.min^{-1}. During the elution step, the valve was switched to the elution position, allowing HNO_3 to be introduced into the system to leach the adsorbed Cu^{2+} from Cu-IIP. The peak height of copper was then recorded by the FAAS detector. The sample and eluent volume was controlled by a loop and 8-way valve.

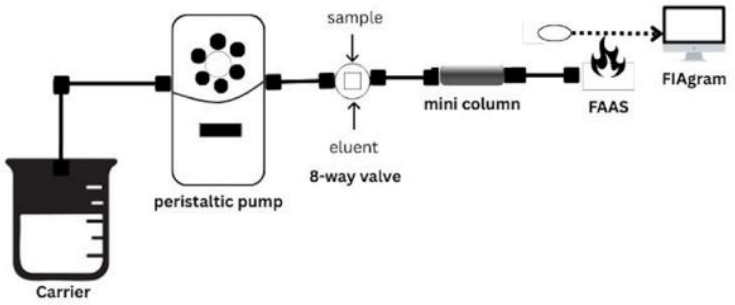


Figure 2. Schematic diagram of the Cu-IIP integrated with FIA-FAAS system.

Results and Discussion

Characterization of Cu-IIP

FTIR Analysis

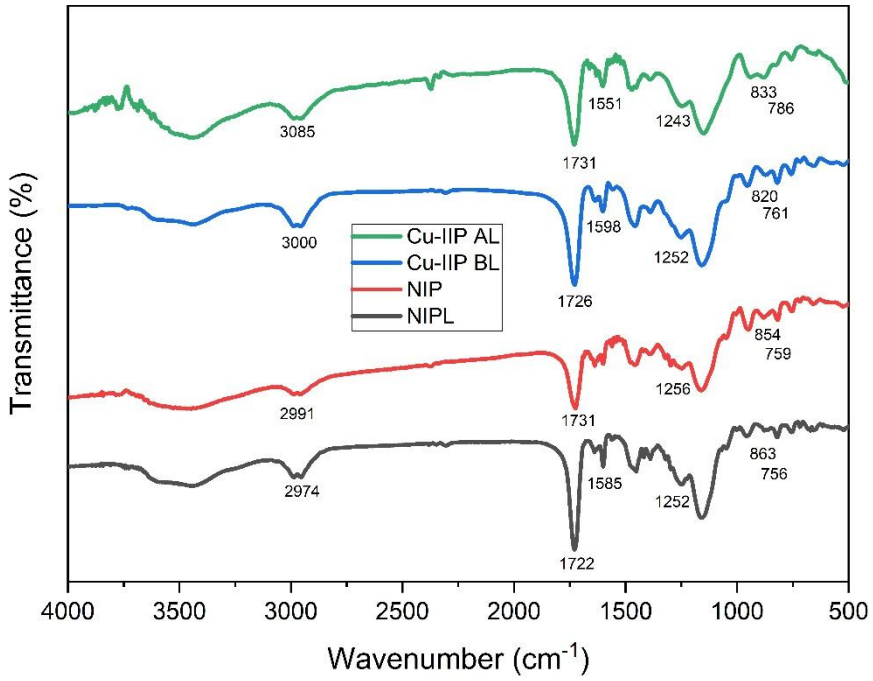
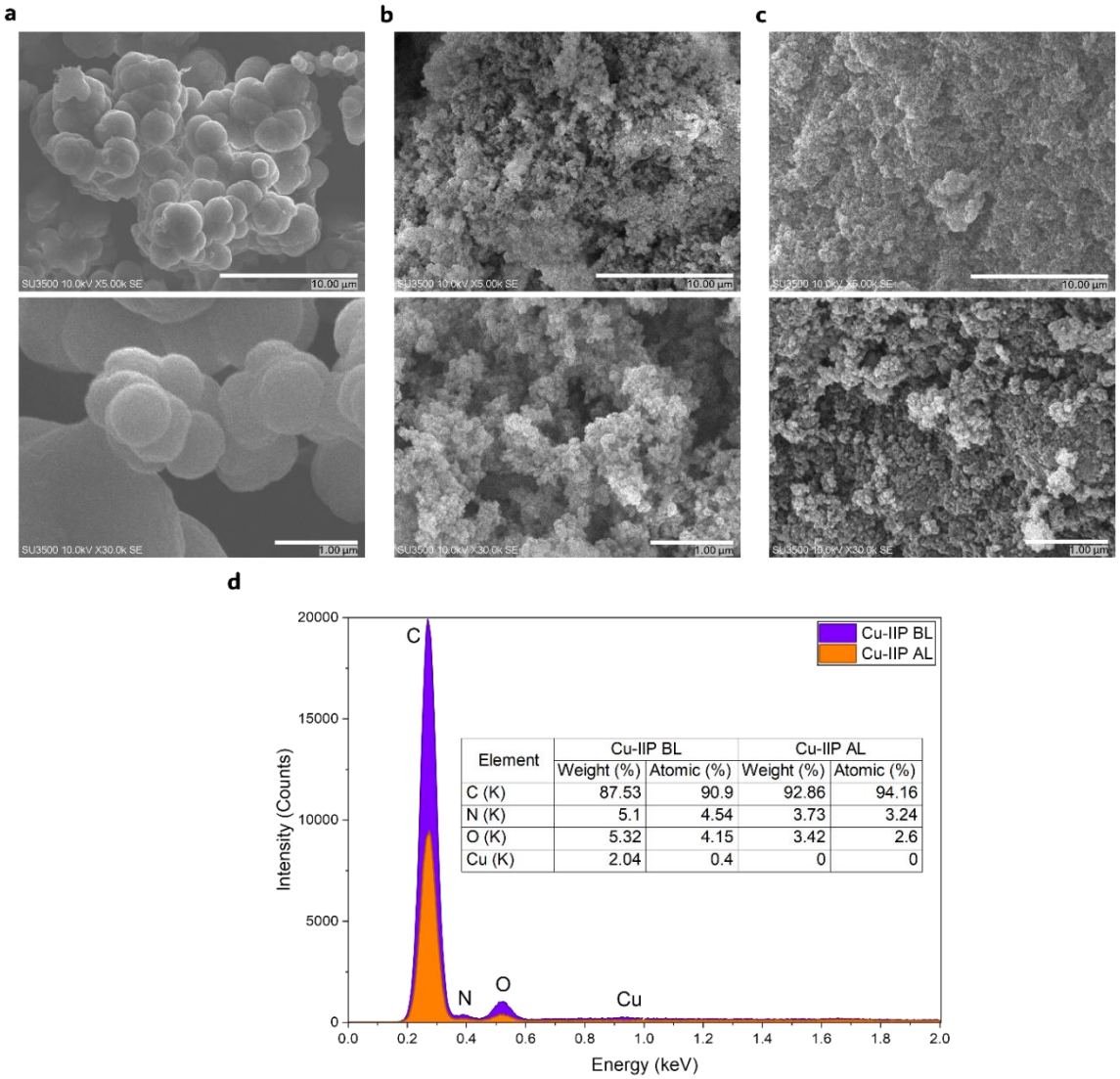


Figure 3. FTIR Characterization Cu-IIP before leaching (BL), Cu-IIP after leaching (AL) and non-imprinted polymers (NIP, NIPL).

FTIR spectroscopy was employed to determine the functional groups present on the surface of the synthesized material. **Figure 3** shows the FTIR spectra of Cu-IIP, NIP, and ligand-loaded NIP-L. The peaks at 1722-1731 cm^{-1} of the synthesized polymers indicated a vibrational stretching of -C=O, which originates from the ester group in EGDMA. The strong bands at 1252-1256 cm^{-1} in all spectra were a stretching vibration adsorption peak of -C-O ester from EGDMA. Following the leaching process, this band exhibited a minor shift from 1726 to 1731 cm^{-1}. In addition, a stretching vibration adsorption peak of -C-O ester group in EGDMA remained essentially unchanged after leaching. The lack of significant changes in these characteristic EGDMA-associated bands demonstrates that the crosslinked polymer backbone was structurally preserved during template removal. These findings indicate that the leaching treatment successfully removed the Cu^{2+} template without causing notable disruption to the crosslinked polymer network. Furthermore, peaks at 1583 cm^{-1}(NIP), 1585 cm^{-1} (NIP-L) and 1598 cm^{-1} (Cu-IIP) were attributed to the stretching vibration adsorption of -N=N- azo from the chromogenic ligand PAR. The slight peak shift from 1585 to 1598 cm^{-1} shows the interaction of the azo group in PAR with the Cu^{2+} ion [33,34], confirming the specific interaction and involvement of the azo group in the imprinting process.



Element	Cu-IIP BL		Cu-IIP AL	
	Weight (%)	Atomic (%)	Weight (%)	Atomic (%)
C (K)	87.53	90.9	92.86	94.16
N (K)	5.1	4.54	3.73	3.24
O (K)	5.32	4.15	3.42	2.6
Cu (K)	2.04	0.4	0	0

Figure 4. SEM image of NIP-L (a) NIP (b) and Cu-IIP after leaching (c) at low (5k) and high (30k) magnification; EDX analysis of Cu-IIP before leaching (Cu-IIP BL) and after leaching (Cu-IIP AL) (d)

These peaks were also attributed to the characteristic band of pyridine ring -C=N- and -C=C- stretching vibration from 4-VP. Moreover, the peaks at 820-854 cm^{-1} corresponded to the -C-H out-of-plane bending in pyridine rings. This pattern indicates the incorporation of 4-VP in the polymer backbone.

SEM EDX characterization

The synthesized material was further characterized using SEM EDX to evaluate the morphology. **Figure 4c** shows that Cu-IIP had a rough, highly porous morphology, whereas NIP-L (**4a**) and NIP (**4b**) had smoother and less defined surfaces. The removal of template Cu^{2+} ions from Cu-IIP forms specific cavities in the polymer matrix [18]. The porous structure of Cu-IIP promotes the diffusion of Cu^{2+} ions, owing to its extensive internal surface area, thereby significantly enhancing adsorption performance relative to non-imprinted materials. **Figure 4d** demonstrates the effective of the Cu^{2+} removal from the Cu-IIP matrix, as confirmed by EDX analysis. Before leaching, Cu-IIP consist of C, N, O and a detectable amount of Cu, confirming the incorporation of Cu^{2+} into the polymer network. Following the leaching process, the complete absence of the Cu signal, indicates efficient elution of the template ions and the formation of vacant imprinted cavities. The slight decrease in nitrogen (from 5.1 to 3.7%) and oxygen (from 5.32 to 3.42%) suggests partial loss or rearrangement of functional ligand during washing, which further supports the creation of accessible binding sites. Meanwhile, the increase in C (from 87.53 to 92.86) could be due to the presence of cavities, which led to most of the polymer chains being exposed.

The compositional change provides strong evidence for successful imprinting and aligns with the observed enhancement in porosity and adsorption performance of Cu-IIP. The EDX analysis aligns with the leaching characterization using AAS of the washing solution in which the concentration of Cu^{2+} was completely removed from the polymer matrix after 5th cycle of washing experiment (**Figure S1**).

Thermogravimetric analysis of Cu-IIP

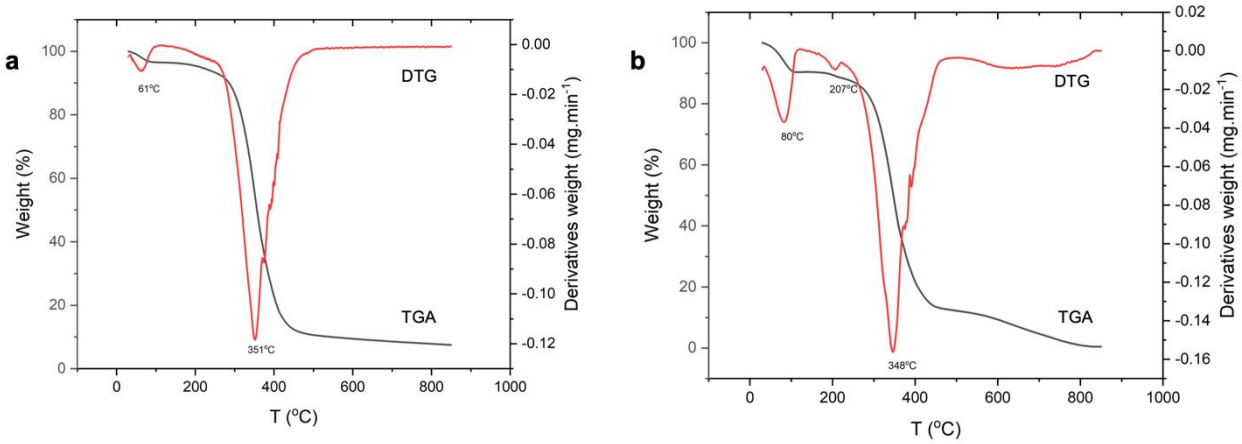


Figure 5. *TGA and DTG curves of Cu-IIP a) before leaching b) after leaching.*

In **Figure 5**, the TGA-DTG profiles show clear differences in thermal behavior before (**5a**) and after removing (**5b**) copper template. A small weight loss from 100 to 97% below 120ºC in Cu-IIP before leaching indicates the removal of moisture. The main degradation occurred at 351°C, where the percent mass of Cu-IIP decrease significantly from 95 to 12%, indicating the degradation of the polymer network. At 900ºC a residual mass 8-10% remained due to the thermally stable inorganic copper species (CuO) [14,35]. After leaching, an additional degradation step was observed at 207 °C, resulting in approximately 16% mass decrease due to structural rearrangement and the loss of coordination stabilization within the imprinted cavities. The major degradation occurred at 348 °C leading to a further decrease in mass to 5% with the final residue reduced to 0-1%. This result confirms the effective of Cu^{2+} removal. The slight shift in the degradation temperatures underscore the role of metal-ligand coordination in enhancing thermal stability prior to template extraction.

Adsorption properties of Cu-IIP

Effect of pH

The optimum pH for Cu^{2+} recognition was evaluated by measuring the maximum adsorption capacity (Qe) over a pH range of 2 to 9 (**Figure 6a**). The maximum adsorption capacity of IIPs increases significantly from pH 2 to 6. The low Cu^{2+} adsorption at pH < 7 is mainly due to the protonation of active sites, leading to a decrease in the active site of hydroxyl group (-OH); in consequence, it reduces the chelating capability with Cu^{2+} in aqueous solution. This phenomenon is in line with the previous research [36]. The maximum adsorption capacity of IIPs is found in the range of pH 6 to 7. At this pH range, the addition of NaOH results in a significant reduction of H^+ in the solution and facilitates deprotonation of oxygen and nitrogen groups, thereby increasing the adsorption capacity [33,37]. When the pH > 7, the adsorption capacity of Cu^{2+} decreases significantly due to the precipitation of Cu^{n+} as $Cu(OH)_n$.

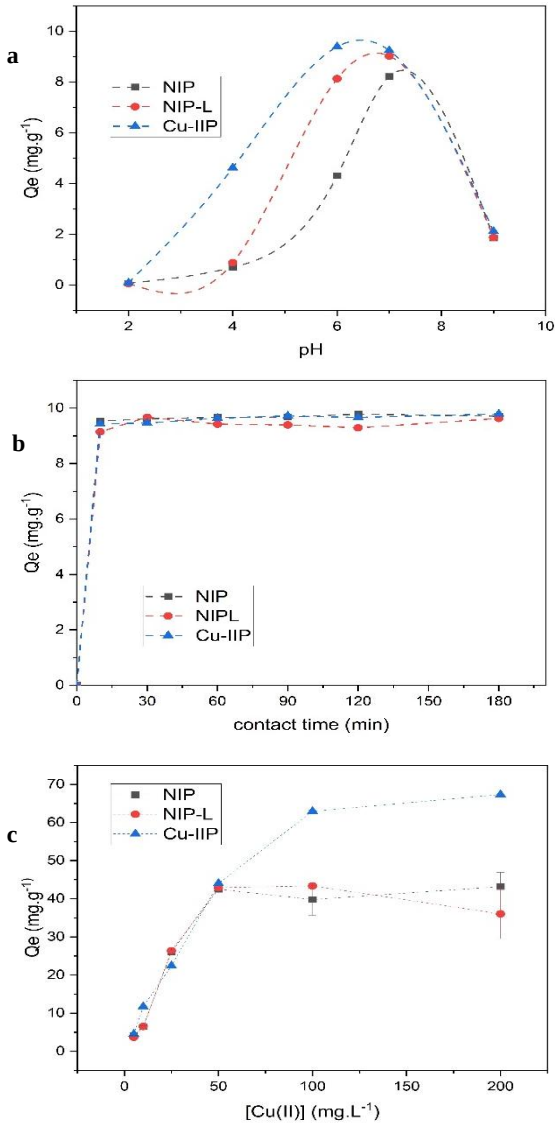


Figure 6. pH effect (a), contact time (b), and Cu^{2+} initial concentration (c).

Effect of contact time

The adsorption kinetics process is notably rapid within the initial 30 min, with over 80% of Cu^{2+} adsorption occurring in the first 10 min (**Figure 6b**). Following the initial phase, the adsorption capacity continued to increase at a slower rate until reaching 90 min, at which point it achieved an equilibrium state. Further increases in contact time do not significantly enhance adsorption efficiency. Notably, a quantitative adsorption of 9.43 mg. g^{-1} was achieved within 10 min for the initial concentration of Cu^{2+} 10 mg. L^{-1}. This rapid uptake is likely due the large pore size, the presence of specific binding active sites, and the rigid pore structure, which facilitate the intraparticle mass transfer during adsorption [19].

Effect of initial Cu^{2+} concentration

Figure 6c illustrates the increments of adsorption capacity of Cu-IIP, NIP, and NIP-L towards the initial concentration of Cu^{2+}. The plot shows that the adsorption capacity increased sharply as the concentration of Cu^{2+} rised from 5 to 100 mg. L^{-1}. However, at the concentration of Cu^{2+} > 100 mg. L^{-1}, the increase in adsorption capacity becomes much slower. This can be explained by the fact that initially all the active sites of IIP were free and available for Cu^{2+} sorption, as adsorption began, the binding sites approached saturation, leading to a slower rate of adsorption. According to the finding on the optimum condition, the maximum adsorption capacity of Cu-IIP, NIP, and NIP-L was 67.32, 43.19, and 36.03 mg. g^{-1} respectively. The maximum adsorption capacity (Qe) value of Cu-IIP shows the higher adsorption

performance than NIP and NIP-L. This is due to the specific recognition sites and spatial structures, which provide greater affinity for target molecules compared to non-imprinted polymers NIP and NIP-L [38].

Adsorption Isotherm

The initial concentration of Cu^{2+} solution plays a significant role in the adsorption characteristics of the imprinted materials. To clarify the isothermal adsorption process, the data for Cu-IIP, NIP and NIP-L were analyzed using the Langmuir, Freundlich, and Temkin models.

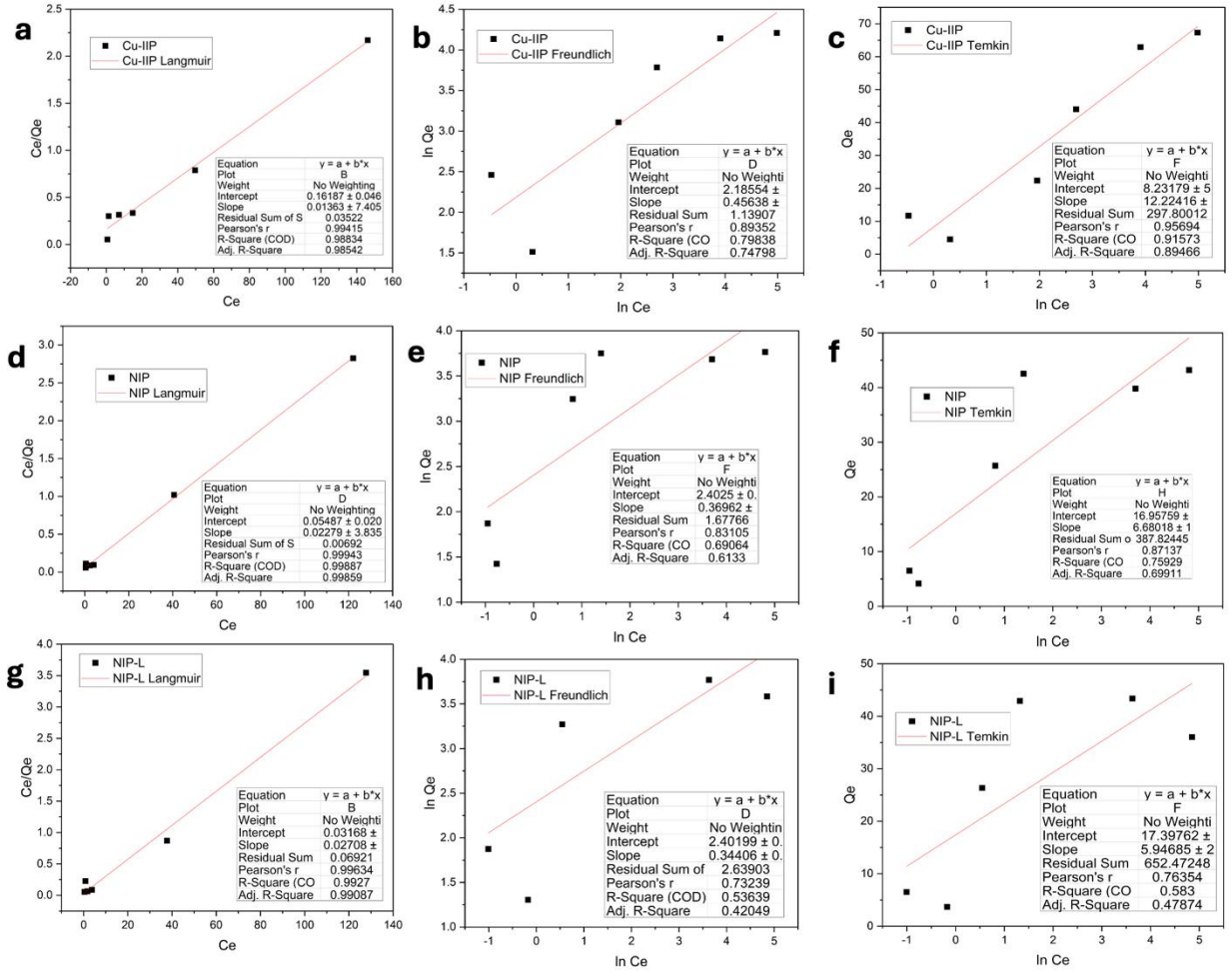


Figure 7. Isotherm adsorption plot of Langmuir, Freundlich and Temkin model for Cu-IIP (a-c), NIP (d-f) and NIP-L (g-i)

Langmuir adsorption isotherm equation:

This model posits that adsorption take places at distinct, homogeneous active sites on the sorbent. These sites exhibited an affinity for monolayer adsorption and no interaction occurs between adsorbed molecules [13,39]. The linear representation of the Langmuir equation is given as follows:

$$\frac{C_e}{q_e} = \frac{1}{q_m} C_e + \frac{1}{K_L q_m} \qquad (4)$$

Where K_L is the Langmuir equilibrium constant (L. mg^{-1}), q_e and q_m are the maximum capacity of adsorbed Cu^{2+} (mg. g^{-1}) and the theoretical maximum adsorption capacity (mg. g^{-1}).

The Freundlich adsorption isotherm equation:

The Freundlich isotherm model posits that the adsorption of the adsorbate onto the adsorbent takes place across multiple surfaces within both the interior and exterior layers of the adsorbent [13,39]. This phenomenon is referred to as a heterogeneous distribution.

$$\ln q_e = \frac{1}{n} \ln C_e + \ln K_F \quad (5)$$

Where K_F is the Freundlich equilibrium constant and n^{-1} is the adsorption strength constant.
Temkin adsorption isotherm equation:
Temkin adsorption isotherms are based on the principle that the heat of adsorption decreases in relation to the increasing coverage of the adsorbent [39,40].

$$q_e = B \ln A + B \ln C_e$$

Where $B = \frac{RT}{b}$, b is the Temkin constant related the heat of sorption, A is the Temkin isotherm constant,

T is the adsorption temperature (K), and R is the molar gas constant.
The isotherm adsorption plot of the Langmuir, Freundlich, and Temkin models is shown in **Figure 7**. From the comparison of the regression coefficient (R^2), it was found that Langmuir > Temkin > Freundlich. Based on the comparison of the equilibrium adsorption capacity q_m values (**Table 1**), it shows that q_m derived from the Langmuir model is closely matched with the experimental data. This indicates that single-layer adsorption was predominant in Cu-IIP, NIP, and NIP-L. The calculated separation factor, denoted as R_L, exhibited values in the range of $0 < R_L < 1$, suggesting favorable adsorption behavior. This observation indicates an effective affinity between the adsorbate and the active sites of the adsorbent as described by the Langmuir model [39]. In alignment with the experimental findings, the maximum adsorption capacities q_m calculated using the Langmuir model showed the same trend (q_mCu-IIP $> q_m NIP > q_m NIP - L$). It confirms the higher affinity of the imprinted polymer for Cu^{2+} ions due to the specific binding sites.

Table 1. Isotherm parameter for adsorption of Cu^{2+} onto Cu-IIP, NIP, and NIP-L.

Isotherm Model	Parameters	Sorbents		
		NIP	NIPL	Cu-IIP
Langmuir	q_{exp}(mg. g^{-1})	43.19	36.03	67.32
	q_m(mg. g^{-1})	43.86	36.90	73.53
	K_L	0.42	0.85	0.08
	R_L	0.012-0.325	0.005-0.189	0.056-0.704
	R^2	0,9989	0,9927	0,9883
Freundlich	K_f ((mg. g^{-1})(Lg^{-1}))	11.05	11.04	8.93
	n	2.71	2.91	2.19
	R^2	0.6996	0.5364	0.7984
Temkin	A	12.66	18.65	1.96
	b	370.88	416.62	202.68
	R^2	0.7593	0.583	0.9157

Thermodynamic study

The thermodynamic study was conducted at temperatures of 298, 308, and 318 K, with the results presented in Figure 8 to provide more profound understanding of the adsorption behavior observed during the experiments. An increase the temperature from 298 K to 318 K demonstrates that the adsorption capacity of Cu-IIP was decreased from 67.32 to 27.97 mg. g^{-1}. The experimental results are consistent with the maximum adsorption capacity (q_m) determined using the Langmuir isotherm model, demonstrating that the q_m value of Cu-IIP decreased with increasing temperature from 73.53 mg. g^{-1} (T 298 K) to 26.88 mg. g^{-1} (T318 K), as presented in **Table S1**.

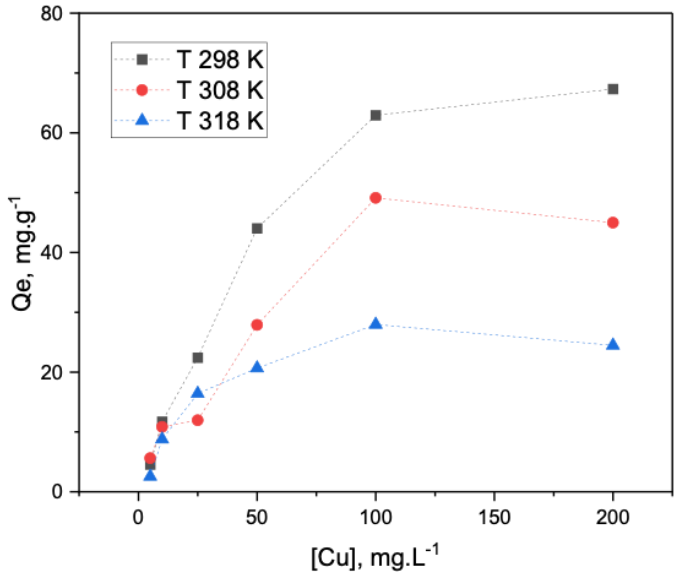


Figure 8. Thermodynamic study of Cu^{2+} adsorption onto Cu-IIP at various temperature.

The reduction in adsorption capacity at higher temperature is likely due to the heat-induced changes in the active binding sites of the imprinted polymer matrix. This alteration compromises both the structural integrity and the specificity of the recognition cavities for the analyte. At elevated temperature, the kinetic energy of metal ions and polymer increases, weakening physical interactions, such as van der Waals forces, between target ions and active sites. This process reduces the stability of the metal ion-polymer complex [40]. The thermodynamic parameters were evaluated at three distinct temperatures (298, 308, and 318 K) by calculating Gibbs free energy (ΔG), enthalpy change (ΔH), and entropy change (ΔS) using the following thermodynamic equations:

$$\Delta G = \Delta H - T\Delta S \quad (7)$$

$$\ln A = -\frac{\Delta H}{RT} + \frac{\Delta S}{R} \quad (8)$$

Table 2. Thermodynamic parameters of Cu^{2+} on Cu-IIP.

Temperature (K)	Δ G (J.mol^{-1})	Δ H (J.mol^{-1})	Δ S (J.mol^{-1})	R^2
298	-1808.15	-16726.11	-50.06	0.8160
308	-1307.55			
318	-806.94			

Table 2 presents the thermodynamic variables calculated at the specific temperatures. The negative values of ΔG observed at the analyzed temperatures demonstrate that the adsorption process is both spontaneous and favorable. As temperature increases, the negative value of ΔG decreases, indicating that the adsorption diminishes with higher temperature [40]. The negative ΔS results from reduces system disorder caused by ion chelation at the active sites of IIP, which stabilize the structure [40,41]. The calculated ΔH values were negative, indicating that the adsorption reaction is exothermic. This observation supports the earlier findings presented in the isotherm studies.

Kinetic Study

Table 3. Pseudo first-order and pseudo-second order kinetic model parameters.

Kinetic model		Sorbents		
		NIP	*NIP-L*	*Cu-IIP*
Pseudo first-order	q_{exp}(mg. g^{-1})	9.71	9.63	9.72
	q_e (cal)	0.21	0.72	0.33
	k_1(min^{-1})	0.006	0.013	0.010
	R^2	0.015	0.720	0.000
Pseudo second-order	q_{exp} (mg. g^{-1})	9.71	9.63	9.72
	q_e (cal)	9.74	9.56	9.72
	k_2(g.mg^{-1}.min^{-1})	3201.68	1028.72	1904.09
	R^2	1.000	0.999	0.999

The kinetic parameter of the adsorption was investigated using Lagergren's pseudo first-order and pseudo second-order equation (**Figure S2**).
Pseudo first-orde:

$$\log(q_e - q_t) = \log q_e - \frac{k_1}{2.303} t \quad (9)$$

Pseudo second-order:

$$\frac{t}{q_t} = \frac{1}{k_2 q_e^2} + \frac{t}{q_e} \quad (10)$$

Where q_t denotes the uptake of Cu^{2+} at time t, k_1 and k_2 correspond to the pseudo first-order (min^{-1}) and pseudo second-order (g.mg^{-1}.min^{-1}) rate constants. The k_1 and k_2 were determined from the intercepts of the corresponding plots of log (q_e - q_t) vs t and t/q_t vs t respectively. These values are compiled in **Table 3**, along with the correlation coefficients, calculated q_e (cal) and experimental q_{exp} values. The higher R^2 values and close alignment between q_e (cal) and q_{exp} for the pseudo-second order rate equation for all sorbents indicate the adsorption of Cu^{2+} onto two surface sites [14].
At low initial Cu^{2+} concentration of 10 mg/L, the q_e value of Cu-IIP, NIP, and NIP-L are nearly identical because most binding sites of all sorbents remain unoccupied, allowing ions to bind without regard to sites selectivity. As the concentration increases, the non-specific sites on NIP become saturated more rapidly, whereas the imprinted cavities on Cu-IIP continue to bind ions efficiently through specific recognition [42]. As a result, the imprinting effect becomes more pronounced at higher Cu^{2+} concentrations, leading to a higher adsorption capacity for Cu-IIP compared to NIP and NIP-L.

The effect of interfering ion

The competitive adsorption experiments were performed using quaternary mixture of Cu^{2+} with interfering ions Pb^{2+}, Cd^{2+} and Zn^{2+} at similar concentration (10^{-4} M). As can be seen from **Table 4** Cu-IIP provided a higher adsorption capacity for Cu^{2+} than that for the three other ions. The selectivity coefficient (k) of Cu^{2+}/Pb^{2+}, Cu^{2+}/Cd^{2+}, and Cu^{2+}/Zn^{2+} were 1.62, 23.00 and 15.99 respectively. These findings confirm the polymer's selective recognition and binding affinity for Cu^{2+} ions in the presence of competing metal ions [37,43].

Table 4. The effect of interfering ion.

Cu-IIP	Metal ions			
	Cu	*Pb*	*Cd*	*Zn*
Q	0.0818	0.0464	0.0027	0.0060
Kd	0.75	0.46	0.03	0.05
k		1.62	23.00	15.99

Preconcentration of Cu^{2+} in Cu-IIP-FIA-FAAS system

Dynamic adsorption capacity

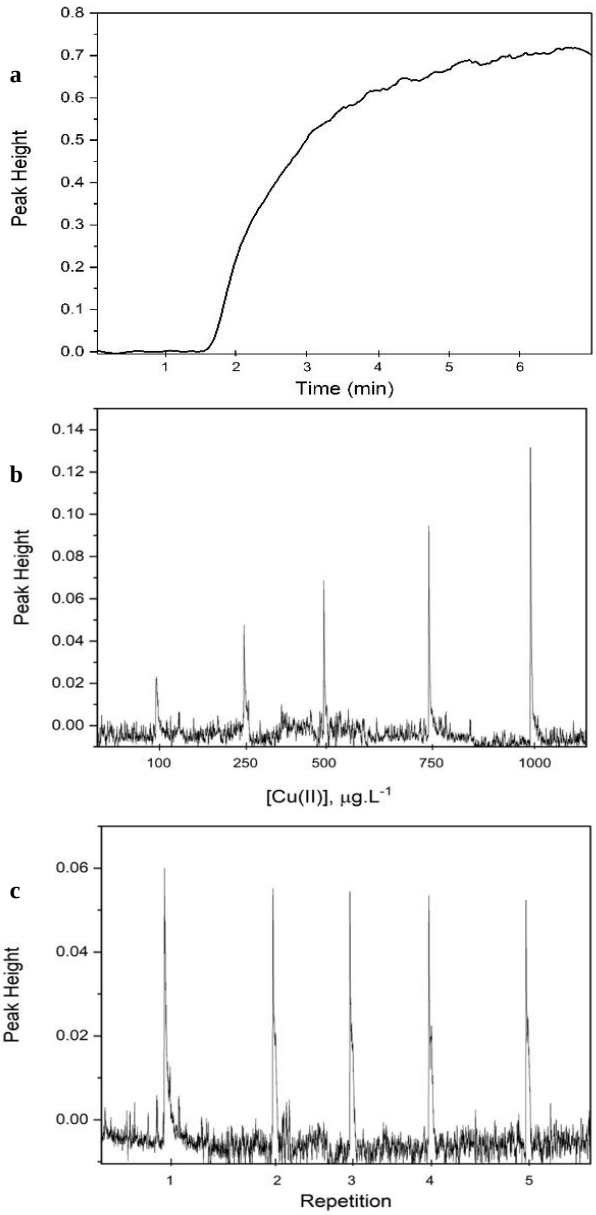


Figure 9. The breakthrough time of Cu-IIP (a), initial concentration of Cu^{2+} (b) and repeatability of Cu^{2+} (c) in the FIA-FAAS system.

The breakthrough volume is defined as the maximum volume of the sample that can pass through the sorbent while still retaining the target analyte. A 50 mg. L^{-1} Cu^{2+} solution was continuously passed through 20 mg Cu-IIP packed in mini column. As loading time increased, the peak height of Cu^{2+} increased sharply due to the accumulation of analyte on the sorbent until equilibrium was reached (**Figure 9a**). Saturation occurred at a breakthrough time of 5.8 minutes with a carrier flow rate of 2.0 $mL.min^{-1}$. The volume breakthrough of the Cu-IIP was 7.6 mL. After this point, Cu^{2+} ions were no longer retained by the Cu-IIP and passed through the column. The dynamic retention capacity of the Cu-IIP was determined to be 29 mg. g^{-1}. This indicates the high number of accessible binding sites and strong

interactions between analyte and the imprinted cavities of the sorbents. Moreover, the large breakthrough volume allows a larger sample volume to be loaded into the FIA system. A 20 mg Cu-IIP in the column can retain up to 580 μg of analyte and thereby the enrichment efficiency and preconcentration factor of the analytical method could be enhanced by increasing the loading volume of the sample [44–46].

As shown in **Figure 9b**, a Fiagram demonstrating the linear correlation between peak height and initial concentration of Cu^{2+} standards solution ranging from 100-1000 μg. L^{-1} using carrier solution at pH 6, 0.5 mL of HNO_3 3M as the eluent and the sample volume of 1.0 mL. The results show a good linearity with R^2 of 0.9919 and a calibration equation of $y = 1.1881x10^{-4}x - 0.01796$ (**Table 5**). Analysis of variance indicates statistical significance for the obtained regression model ($p<0.001$).

$$EF = \frac{S_{Cu-IIP-FIA-FAAS}}{S_{Cu(II)-FAAS}} \quad (11)$$

$$CE = \frac{f}{60} x\ EF \quad (12)$$

$$CI = \frac{V_s}{EF} \quad (13)$$

An EF value (eq. 11) of 2.17 demonstrates effective enhancement of the analytical signal, confirming that the preconcentration method increases sensitivity [46,47]. A CE value (eq. 12) of 1.08 min^{-1} indicates that the processes analyte at an efficient rate while maintaining signal enhancement. The CI value (eq. 13) of 2.53 reflects a small volume of analyte required for enrichment. These results indicate that Cu-IIP-FIA-FAAS system achieves a balance among sensitivity, speed and sample consumption supporting its suitability for routine analysis of Cu(II) in the samples.

Table 5. Linear fit parameter of Cu(II) measurement with preconcentration in FIA-FAAS system and without preconcentration.

Cu^{2+} measurement Parameters	Cu-IIP-FIA system	Without preconcentration
a	0.01796	-0.003
k	$1.1881x10^{-4}$	$5.478x10^{-5}$
R^2	0.9919	0.9998
$[Cu^{2+}]$ range (mg. L^{-1})	100-1000	1000-5000

LoD and LoQ were determined by adding 3σ and 10σ of the blank signal respectively to the mean of blank signal, where σ denotes the standard deviation of signal from blank analysis (n=30). The LoD and LoQ of the proposed method were found to be 3.07μg.L^{-1} and 9.03 μg. L^{-1}.

Repeatability of the proposed method was assessed using five consecutive measurements at a Cu^{2+} concentration of 500 μg. L^{-1} (**Figure 9c**). The result demonstrates a good precision with a CV of 3.53% under specific analysis condition. Compared to the predicted CV from the Horwitz equation (6-7%) at this concentration, the observed CV is substantially lower indicating good repeatability.

Application to determination of Cu^{2+} in water sample

The proposed method was used to the measure Cu^{2+} in tap water sample derived from groundwater (Parongpong, Bandung West Java Indonesia). **Table 6** shows that spike recovery experiments at concentration level of 200 and 500 μg.L^{-1} produces recoveries ranging from 102.91-105.53%, which indicates a high recovery and minimum matrix interference. These results are within the acceptable range for trace analysis and confirm the reliability of the proposed method for Cu^{2+} determination in tap water.

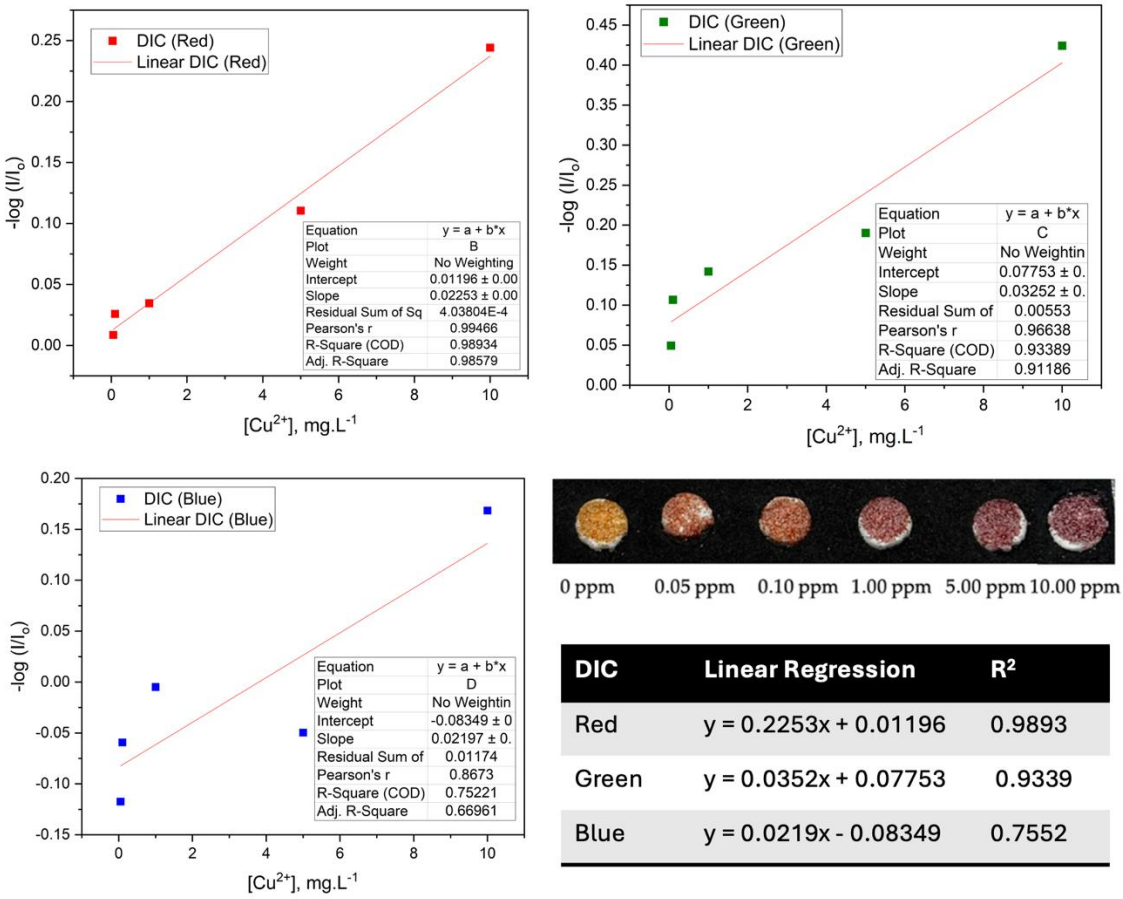
Table 6. Application of Cu^{2+} determination in tap water sample.

Sample	Cu^{2+} added		Recovery %
	Spiked	*Found*	
TW-GW	0	2.2	
	200	208.1	102.91
	500	530	105.53

The analytical characteristics of the proposed method for preconcentration and Cu^{2+} determination were summarized in **Table S2**.

Adsorption recognition mechanism and DIC analysis

Ligand increases the recognition process for template molecules and forms immobilize covalent/ noncovalent bonds which significantly affects the selectivity [47]. 4-(2-pyridylazo) resorcinol is often used in photometric analysis of metal ions, the alteration of Cu-IIP color before and after metal adsorption is intriguing to be studied further.



DIC	Linear Regression	R^2
Red	y = 0.2253x + 0.01196	0.9893
Green	y = 0.0352x + 0.07753	0.9339
Blue	y = 0.0219x - 0.08349	0.7552

Figure 10. DIC analysis of color-shiftable Cu-IIP.

Figure 10 shows that the binding interaction between Cu^{2+} ions and Cu-IIP containing the chromogenic ligand PAR results in a noticeable color change. A study was conducted to measure Cu^{2+} concentration in a solution using the DIC (Digital Image Colorimetry) method. This approach has proven to be easy to operate, rapid, and cost-effective [48,49].

This color was attributed to metal-to-ligand charge transfer (MLCT) transitions. Cu^{2+} was then removed from the polymer, leaving behind the trapped PAR ligand within the polymer network (yellow color). The characteristic reddish-purple color was restored after Cu^{2+} adsorption due to the re-complexation of the Cu-PAR in the imprinted cavities. The relationship between Cu concentration and the intensity of each RGB component was determined by using the following equation:

$$Intensity\ (I_{RGB}) = -\log \frac{I_{Cu-IIP}}{I_b} \quad (11)$$

Where I_{Cu-IIP} is the color intensity of RGB components in Cu-IIP (ranging from 0 to 255) and I_b is the RGB color intensity of blank. A linear fit was performed on the relationship between Cu concentration and the color intensity of the RGB components. Compared to the green and blue components, the red

component exhibited the highest degree of variability, with an R^2 value of 0.9893 in Cu^{2+} concentration range of 0.05-10 mg. L^{-1}. The LoD of this method was 0.02 (n=7) mg. L^{-1} and the LoQ was 0.08 mg. L^{-1}. Therefore, red can be selected as the test color for DIC analysis.

Comparative study of Cu-IIP with previous work

Preconcentration of Cu^{2+} in water-based samples reported by another research group was summarized in **Table 7**. According to the results, Cu-IIP is introduced selective sorbent for preconcentration, employing a significantly reduced sample volume compared to previously reported method. While most preconcentration techniques require large sample volumes (20-1000 mL) to achieve enrichment factors, the proposed method achieves excellent recovery (102.91-105.53%) and reliable selectivity with a much smaller sample volume.

Table 7. Comparative study of synthesized Cu-IIP with previous work.

Material	Method	V sample (mL)	EF	Recovery (%)	Ref
Cu-IIP	SPE	50	24	75-94	[13]
Cu(II)-IIPs	batch	50	NI	98-101	[14]
Cu-IIP polymeric beads	SPE	25-1000	100	>97	[18]
Fe_3O_4@SiO_2@IIP	batch	100	200	97-98	[37]
Poly(protoporphyrin-co-vinyl-pyridine)	FIA	14	41,7	91.7-101.9	[50]
RH-CIIP	SPE	50	NI	NI	[51]
Cu-IIP	FIA	1	2,2	102.9-105.5	**This work**

Conclusion

A novel study of a dual-functional Cu-IIP serving as both a preconcentration sorbent and a colorimetric sensing platform was conducted in this research. Cu-IIP has good adsorption performance for Cu^{2+} with the relatively high adsorption capacity 67.32 mg. g^{-1}. The imprinting cavities enable selective enrichment of Cu^{2+} ions, while the immobilized chromogenic.
ligand allows direct visual detection through color change in the presence of Cu^{2+} ions. The proposed preconcentration system Cu-IIP-FIA-FAAS demonstrates potential with good linearity over a wide range concentration of Cu^{2+} 100-1000 μg. L^{-1} with R^2 0.9919, a low detection limit (LoD) of 3.07 μg. L^{-1}, and a satisfactory precision 3.53%. The minimal consumption of sample (1.00 mL) and reagents underscores its suitability as an environmentally friendly method that aligns with green chemistry principle. Moreover, the color change observed in Cu-IIP upon adding the sorbents to the Cu^{2+} solution allows for both direct and indirect measurements for qualitative and quantitative analysis of Cu^{2+}.

Acknowledgment

This research was supported by Indonesian Education Scholarship (Beasiswa Pendidikan Indonesia, BPI), Center for Higher Education Funding and Assessment (PPAPT), Ministry of Higher Education and Indonesian Endowment Fund for Education (LPDP) under grant number 2022209090777.

Author Contributions

Dita Arifa Nurani: conceptualization, design the experiments, investigation, data management, writing original manuscript. **Untung Triadhi:** method development, supervision, a manuscript revision. **Dian Ayu Setyorini:** visualization, data interpretation, a manuscript revision **Muhammad Bachri Amran:** conceptual development, methodology design, supervision, manuscript review.

References

[1] V. Singh, G. Ahmed, S. Vedika, P. Kumar, S.K. Chaturvedi, S.N. Rai, E. Vamanu, A. Kumar, Sci. Rep. 14 (2024) 7595.
[2] A. Alengebawy, S.T. Ahmed, R. Qureshi, W. Sundas, M.Q. Wang, Toxics 9 (2021) 42.
[3] S. Kotnala, S. Tiwari, A. Nayak, B. Bhushan, S. Chandra, C.R. Medeiros, H.D.M. Coutinho, Sci. Total Environ. 987 (2025) 179785.
[4] Y. Zou, S. Wu, X. Xu, X. Tan, S. Yang, T. Chen, J. Zhang, S. Li, W. Li, F. Wang, Int. Immunopharmacol. 133 (2024) 112075.
[5] R. Manne, M.M.R.M. Kumaradoss, R.S.R. Iska, A. Devarajan, N. Mekala, Appl. Water Sci. 12 (2022) 27.
[6] S. Joshi, R.K. Srivastava, Environ. Monit. Assess. 191 (2019) 615.
[7] M. Li, M.Y. Li, C.G. Feng, Q.X. Zeng, Appl. Surf. Sci. 314 (2014) 1063–1069.
[8] M.A. Darweesh, M.Y. Elgendy, M.I. Ayad, A.M.M. Ahmed, N.M.K. Elsayed, W.A. Hammad, S. Afr. J. Chem. Eng. 40 (2022) 10–20.
[9] M. Shahrashoub, S. Bakhtiari, Microporous Mesoporous Mater. 311 (2021) 10692. https://doi.org/10.1016/j.micromeso.2020.110692.
[10] G. Duan, X. Li, X. Ma, W. Zhong, S. Wang, Sci. Total Environ. 864 (2023) 160984.
[11] Z. Wang, W. Xu, F. Jie, Z. Zhao, K. Zhou, H. Liu, Sci. Rep. 11 (2021) 16878.
[12] T.C. Egbosiuba, A.S. Abdulkareem, J. Mater. Res. Technol. 15 (2021) 2848–2872.
[13] P. Cao, V. Pichon, C. Dreanno, K. Boukerma, N. Delaunay, Talanta 256 (2023) 124295.
[14] T. Zhang, X. Yue, K. Zhang, F. Zhao, Y. Wang, K. Zhang, Hydrometallurgy 169 (2017) 599–606.
[15] Y. Pan, F. Zhang, W. Gao, Y. Sun, S. Zhang, H. Lian, L. Mao, Chin. J. Chromatogr. 40 (2022) 979–987.
[16] F.A. Mustafai, A. Balouch, Abdullah, N. Jalbani, M.I. Bhanger, M.S. Jagirani, A. Kumar, A. Tunio, Eur. Polym. J. 109 (2018) 133–142.
[17] Y. El Ouardi, A. Giove, M. Laatikainen, C. Branger, K. Laatikainen, J. Environ. Chem. Eng. 9 (2021) 106548.
[18] S. Mishra, A. Tripathi, J. Environ. Chem. Eng. 8 (2020) 103656.
[19] S. Rais, A. Islam, I. Ahmad, S. Kumar, A. Chauhan, H. Javed, Food Chem. 334 (2021) 127656.
[20] A. Kocyła, A. Pomorski, A. Krężel, J. Inorg. Biochem. 152 (2015) 82–92.
[21] D.K. Singh, S. Mishra, Chromatographia 70 (2009) 1539–1545.
[22] B.-C. Iacob, A.E. Bodoki, L. Oprean, E. Bodoki, in: C. Saravanan, B. Biswas (Eds.), Ligand, IntechOpen, London, 2018, p. 1–28.
[23] X. Cai, J. Li, Z. Zhang, F. Yang, R. Dong, L. Chen, ACS Appl. Mater. Interfaces 6 (2014) 15739–15748.
[24] A. Cihanbay, H. Sari, F.N. Al-Obaidi, H. Atabey, Russ. J. Inorg. Chem. 69 (2024) 1165–1172.
[25] E.Y. Bivián-Castro, A. Zepeda-Navarro, J.L. Guzmán-Mar, M. Flores-Alamo, B. Mata-Ortega, Polymers 15 (2023) 1186.
[26] Y. Jiang, B. Tang, P. Zhao, M. Xi, Y. Li, J. Inorg. Organomet. Polym. Mater. 31 (2021) 4628–4636.
[27] T.P. Rao, R. Kala, S. Daniel, Anal. Chim. Acta 578 (2006) 105–116.
[28] S. Daniel, R.S. Praveen, T.P. Rao, Anal. Chim. Acta 570 (2006) 79–87.
[29] T. Bicim, M. Yaman, J. AOAC Int. 99 (2016) 1043–1048.
[30] F. Fereidoonipour, H.R. Rajabi, New J. Chem. 41 (2017) 8828–8836.
[31] D.F. Moreira Naves, C. dos Reis Feliciano, M.G. Santos, Anal. Chim. Acta 1296 (2024) 342308.
[32] A. Lamaoui, J.J. García-Guzmán, A. Amine, J.M. Palacios-Santander, L. Cubillana-Aguilera, in: S. Thomas, M.P. Patil (Eds.), Molecularly Imprinted Polymer Composites: Synthesis, Characterisation and Applications, Elsevier, Amsterdam, 2020, p. 49–91.
[33] D. Qi, H. Zhang, Z. Zhou, Z. Ren, J. Environ. Chem. Eng. 11 (2023) 110804.
[34] M. Behbahani, P.G. Hassanlou, M.M. Amini, H.R. Moazami, H.S. Abandansari, A. Bagheri, S.H. Zadeh, Food Anal. Methods 8 (2015) 558–568.
[35] M. Boudias, A. Gourgiotis, C. Cazala, V. Pichon, N. Delaunay, Adv. Sample Prep. 5 (2023) 100049.
[36] T. Zhang, X. Yue, K. Zhang, J. Li, C. Zhu, L. Zhang, W. Chen, Mater. Des. 107 (2016) 372–377.
[37] Z. Dahaghin, H.Z. Mousavi, L. Boutorabi, J. Mol. Liq. 243 (2017) 380–386.
[38] Y. Sun, Y. Gu, P. Zhang, J. Hazard. Mater. 424 (2022) 127735.
[39] M.A. Al-Ghouti, D.A. Da'ana, J. Hazard. Mater. 393 (2020) 122383.
[40] E. Ghorbani, S. Bagheri Renani, P. Zahedi, New J. Chem. 48 (2024) 9794–9804.
[41] L. Zhou, C. Shang, Z. Liu, G. Huang, A.A. Adesina, J. Colloid Interface Sci. 366 (2012) 165–172.
[42] J. Long, X. Luo, X. Yin, X. Wu, J. Environ. Chem. Eng. 4 (2016) 4776–4785.
[43] N. Ambarsari, M.A. Zulfikar, M.B. Amran, Anal. Bioanal. Chem. Res. 10 (2023) 71–86.
[44] Y. Li, C. Wang, J. Zhao, X. Liu, M. Ma, A. Gao, K. Sun, Anal. Methods 17 (2025) 5807–5830.
[45] U. Haseen, S. Kapoor, R.A. Khan, B.H. Koo, RSC Adv. 15 (2025) 8729–8739.
[46] M.B. Amran, N. Ambarsari, M.A. Zulfikar, A. Indrawati, R. Rusnadi, S. Hamdi, J. Anal. Test. 8 (2024) 180–190.
[47] H. Liu, D. Kong, W. Sun, Q. Li, Z. Zhou, Z. Ren, Chem. Eng. J. 303 (2016) 348–358.
[48] G. de Carvalho Oliveira, C.C.S. Machado, D.K. Inácio, J.F. da Silveira Petruci, S.G. Silva, Talanta 241 (2022) 123244.
[49] Y. Fan, J. Li, Y. Guo, L. Xie, G. Zhang, Measurement 171 (2021) 108829.
[50] F.A. Cajamarca Suquila, L.A. Bertoldo, E. Lins, C.R.T. Tarley, Separations 10 (2023) 122.
[51] Y. Gao, R.Y. Zhou, L. Yao, W. Yin, J.X. Yu, Q. Yue, Z. Xue, H. He, B. Gao, J. Hazard. Mater. 424 (2022) 127203.